metals

MDPI

Article

Influence of Single- and Double-Aging Treatments on the Mechanical and Corrosion Resistance of Alloy 625

Barbara Rivolta *, Riccardo Gerosa and Davide Panzeri

Department of Mechanical Engineering, Politecnico di Milano, Via La Masa 1, 20156 Milan, Italy; riccardo.gerosa@polimi.it (R.G.); davide.panzeri@polimi.it (D.P.)
* Correspondence: barbara.rivolta@polimi.it

Abstract: Nickel–chromium–molybdenum Alloy 625 exhibits an excellent combination of mechanical properties and corrosion resistance. However, the high-temperature plastic deformation process and the heat treatment represent critical aspects for the loss in mechanical strength by grain coarsening. This detrimental behavior is worsened by the absence of phase transformation temperatures. However, the chemical composition permits slow precipitation-hardening response upon single aging. Therefore, when the soft- or solution-annealed condition is associated with insufficient mechanical properties, this potentiality can be exploited to improve the mechanical strength. Since the γ'' precipitation can be accelerated by double-aging treatment, different time–temperature combinations of double aging at 732 °C and 621 °C are investigated. The simultaneous precipitation of intergranular carbides can dramatically affect the corrosion resistance. Such an undesired phenomenon occurs very quickly at 732 °C, but it is obtained only after very long exposure times at 621 °C. For this reason, a performance chart is developed to compare all the tested conditions. In particular, single aging at 621 °C for 72 h and 130 h are associated with an acceptable combination of mechanical and corrosion properties. Double aging permits a conspicuous acceleration of the aging response. For instance, with double aging at 732 °C 3 h and 621 °C 72 h, it is possible to obtain the same mechanical properties of single aging at 621 °C for 260 h. Such acceleration is accompanied by a more critical corrosion behavior, especially because of the primary step. However, even after its optimization, none of the tested conditions were acceptable.

Keywords: Alloy 625; aging treatment; mechanical strength; corrosion resistance

check for updates

Citation: Rivolta, B.; Gerosa, R.; Panzeri, D. Influence of Single- and Double-Aging Treatments on the Mechanical and Corrosion Resistance of Alloy 625. *Metals* **2024**, *14*, 823. https://doi.org/10.3390/met14070823

Academic Editors: Yongquan Ning, Yanhui Liu and Bingchao Xie

Received: 19 June 2024
Revised: 15 July 2024
Accepted: 16 July 2024
Published: 17 July 2024

Copyright: © 2024 by the authors. Licensee MDPI, Basel, Switzerland. This article is an open access article distributed under the terms and conditions of the Creative Commons Attribution (CC BY) license (https://creativecommons.org/licenses/by/4.0/).

1. Introduction

Nickel–chromium–molybdenum–niobium Alloy 625, patented in 1964 by H. L. Eiselstein and J. Gadbut, provides excellent mechanical and corrosion properties thanks to the presence of high amounts of chromium, molybdenum, and niobium [1,2]. The excellent potentialities of this material are mainly exploited for applications in the oil and gas and automotive fields [3]. This alloy grade was selected for this research work because of its popularity and extensive adoption in the offshore oil and gas field to produce forged components, such as pipes, valves, hubs, flanges, disks, and spheres. Considering the difficulties in maintaining a fine grain size during processing [4] and heat treatment [5], this paper provides useful information about the possibility of recovering insufficient mechanical properties via tailored aging treatments when excessive grain coarsening is present. The ASTM B446 standard [6] reports two possible heat-treating conditions for this material: soft annealing and solution annealing. No aging treatments are currently prescribed by the ASTM B446 standard [6]. For applications below 600 °C where a good combination of tensile strength and corrosion resistance is required, soft annealing is recommended, and it requires a minimum temperature of 871 °C [6]. The solution-annealing treatment is suggested for high creep strength, and it is performed at a minimum of 1093 °C for applications above 600 °C [6]. In the soft-annealed condition, this alloy shows a fully austenitic

microstructure with a heterogeneous distribution of primary carbides and nitrides which are induced by the solidification process [2,7]. These compounds are mainly enriched in niobium and titanium, which are depleted from the surrounding regions. The process- and service-induced thermal exposure above 600 °C can activate complex precipitation phenomena that can significantly alter both the mechanical properties and the corrosion resistance [2,8]. However, the formation of hardening phases can be exploited to recover insufficient mechanical properties in the solution- or soft-annealed condition [6]. The time–temperature–precipitation (TTP) diagram of this alloy is shown in Figure 1 [2]. The precipitate phases reported in the literature for this alloy are MC, M_6C, and $M_{23}C_6$ metal carbides and intermetallic phases, normally γ'', δ, and Laves [2,9,10]. The precipitation of intergranular carbides and intermetallic phases induces sensitization and reduction in toughness and deformability. The susceptibility to intergranular corrosion is increased by the formation of intergranular carbides rich in chromium and molybdenum. In fact, these alloying elements are depleted from the surrounding regions, preventing the auto-passivation mechanism [2,8,11,12]. Moreover, intergranular cracking is favored by the formation of intergranular films of carbides resulting in a reduction in toughness [13]. In this material, the presence of insufficient mechanical properties is a common issue, and it is related to the difficulty in retaining a fine-grained structure during processing and heat treatment. In fact, regarding the high-temperature plastic deformation process, the optimal region of temperatures and strain rates is very restricted. For this reason, the plastic deformation procedure should be carefully designed, but very often, depending on the available equipment and the component geometry, the recrystallization process is not optimal. Moreover, grain refinement via heat treatment cannot be obtained because of the absence of phase-transformation temperatures. Furthermore, these detrimental characteristics are worsened by the fact that both the soft- and the solution-annealing treatments are inevitably associated with grain coarsening, which degrades the overall mechanical performance [5]. Therefore, because the mechanical properties are directly related to the grain size [5], the heat treatment parameters should be tuned as to provide the best compromise between the solubilization level, which affects the corrosion resistance, and the grain size, which determines the mechanical strength. The possibility to recover the strength loss induced by excessive grain coarsening by aging treatment is very useful, but this requires a careful optimization to find the best balance between the mechanical and corrosion properties and the heat treatment time, which directly affects costs and energy consumption. The ordered intermetallic γ'' Ni_3Nb hardening phase is obtained upon aging from 600 °C to 800 °C [2,9,14]. In the literature, Moore et al. and Suave et al. [8,15,16] investigated the single-aging response in temperature range from 600 °C to 800 °C and from 550 °C to 900 °C, respectively. However, the hardening effect was significant only after very long exposure times, which are typically not compatible for industrial applications. This strength improvement is generally obtained at the expense of deformability and corrosion resistance, which is worsened by the precipitation of Cr-rich carbides.

Starting from the first experimental results on this topic published in our previous work (Rivolta et al. [17]), this research paper is aimed at investigating additional non-standard single- and double-aging conditions to improve the accuracy and the completeness of the analysis of the precipitation-hardening response given in [17], especially with longer aging times. The development of this additional work also rises from the necessity to find other acceptable conditions with more satisfying mechanical properties. Moreover, in the literature, few data are available about double aging and the influence of the aging treatment on the corrosion properties. For instance, Eiselstein and Tillack [1] provided a preliminary investigation about the adoption of a nucleation treatment to accelerate the age-hardening response at 650 °C. In this work, significant findings compared to [17] are reported. In fact, based on the results published in [17], only one condition was acceptable, but its mechanical strength was too close to the minimum standard requirement. In the current paper, a new condition in the acceptability region of the performance chart (621 °C 130 h) was found with more satisfying mechanical strength in comparison to the 621 °C 72 h

condition identified in [17]. Furthermore, compared to our previous work [17], significant acceleration of the age-hardening response at 621 °C after 72 h was identified. Moreover, the new tensile tests reported in this paper permit us to improve the accuracy of the relationships between the hardness and the tensile properties given in [17]. Regarding the corrosion tests, this work provides additional results about the variation in the corrosion rate increasing the aging time at 621 °C. Moreover, in our previous work [17], the influence of the primary aging time in the case of double aging was not investigated. In this paper, with fixed secondary aging time, different primary aging times are tested to check if proper limitations of this exposure are sufficient to improve the corrosion resistance. The strength improvement allowed by single- and double-aging treatments can be exploited to reduce the consumption of resources and the carbon footprint thanks to the thickness and mass reduction. Moreover, the reduction in the component weight enables lower fuel consumption and operative costs.

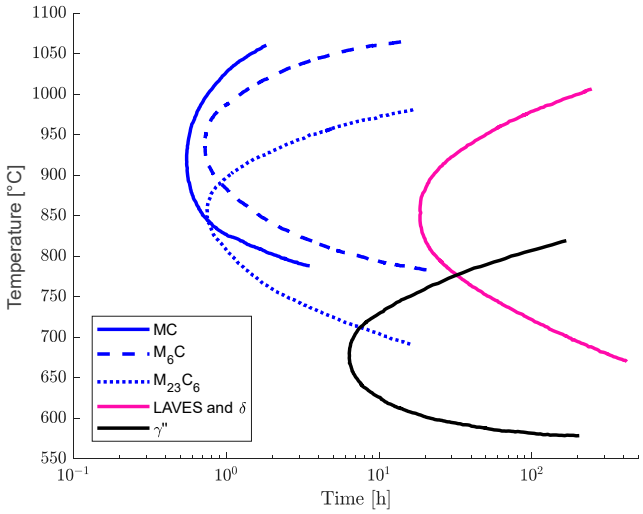


Figure 1. Experimental TTP diagram of the alloy investigated in this work. Adapted from Refs. [2,17].

As previously described, retaining a fine grain size during processing and heat treatment is a critical aspect for this alloy. Therefore, when the mechanical properties in the as-solubilized condition are not sufficient compared to the standard prescriptions because of excessive grain coarsening, the possibility of exploiting the aging treatment to obtain a strength improvement can be beneficial to recover a component. However, considering that the corrosion resistance is typically reduced upon aging because of sensitization, this work aimed at identifying the feasibility region (if any) where both the mechanical and the corrosion properties are acceptable. In this work, the aging treatment was studied with hardness, tensile, and corrosion tests for both single and double aging with different time-temperature combinations. Its investigation was developed starting from the double aging recommended for alloy CarTech® Custom Age 625 PLUS® [18,19]. In this case, compared to the conventional Alloy 625, a higher titanium content is present to promote the formation of γ'' Ni_3Nb precipitates [9,18,19]. Regarding this variant, the best combination of age-hardening response and corrosion resistance is obtained with double aging at 732 °C for 8 h and 621 °C for 8 h after soft-annealing treatment at 1038 °C [18,19]. The resistance to intergranular corrosion was analyzed in selected aging conditions according to the ASTM G28-A standard [20]. The corrosion rate limit was considered equal to 1.20 mm/year. The experimental results were finally reported in a performance map to provide a graphical and more effective overview of the relationship between the mechanical properties and the corrosion resistance after aging.

2. Materials and Methods

The material investigated in this work is a forged and untreated Alloy 625 rod with diameter of 60 mm. The soft-annealing and the single- and double-aging treatments were carried out in a laboratory furnace operating in atmospheric air. The tensile specimens were machined in the longitudinal direction. Regarding the metallographic and hardness samples, after grinding and polishing, etching was carried out in five parts HCl diluted in one part 30% H_2O_2 for 10 s [18,21,22]. The reagents were produced by CARLO ERBA Reagents s.r.l., Cornaredo, Mi, Italy. The microstructural analyses were performed using a Leica (model DMR, sourced from Leica Microsystems S.r.l., Buccinasco, Italy) light optical microscope and a Zeiss (model SIGMA 500, sourced from Carl Zeiss S.p.A., Milano, Italy) scanning electron microscope. The HV30 Vickers hardness tests were conducted using a Wolpert Testor 930 hardness tester (sourced from Wolpert, Ludwigshafen am Rhein, Germany) in accordance with the EN ISO 6507 standard [23]. In each tested condition, at least five hardness measurements were carried out. The tensile tests were performed using cylindrical proportional specimens with diameter of 8 mm and gauge length of 40 mm. The tensile tests were carried out with an INSTRON model 4507 machine (sourced from Instron, Pianezza, TO, Italy) according to the EN ISO 6892 standard [24]. The intergranular corrosion tests were performed in a solution of ferric sulfate, $Fe_2(SO_4)_3$, and sulphuric acid, H_2SO_4, for 120 h, in accordance with the ASTM G28—Method A standard [20]. The reagents were produced by CARLO ERBA Reagents s.r.l., Cornaredo, Mi, Italy. After cutting with silicon carbide cut-off wheels, the corrosion specimens were fully descaled and polished using wet 80-grit and 120-grit abrasive papers and then degreased and dried. After testing, selected corrosion specimens were cut and mounted in a thermosetting phenolic resin and mirror polished to observe the corroded profile and characterize the corrosion mechanism.

The mechanical strength requirements considered for the evaluation of acceptability were taken from the ASTM B446 standard [6]. For the corrosion resistance, a maximum corrosion rate of 1.20 mm/year was considered. SEM and chemical EDXS analyses were carried out to better investigate the relationship between the microstructural constituents and the corrosion properties. The qualitative EDXS chemical analyses were performed using the OXFORD Altee Energy—Advanced detector (sourced from Oxford Instruments, Wiesbaden, Germany). The bulk chemical composition was investigated by OES spectroscopy. The results are reported in Table 1. Based on the requirements of the ASTM B446 standard [6], the chemical composition is acceptable.

Table 1. Chemical composition by OES spectroscopy of material investigated in this paper.

	Ni	Cr	Mo	Nb	Fe	Mn	Ti	Al	C	Si	P	S
wt. %	62.3	20.4	8.50	3.59	4.41	0.09	0.30	0.20	0.04	0.17	<0.01	<0.01

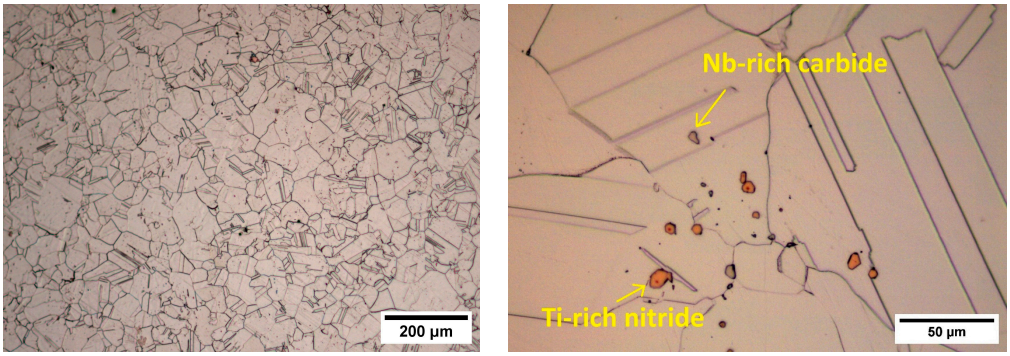
Before the aging treatment, all the samples and specimens were soft annealed at 1038 °C for 0.5 h and water-quenched. The hardening response upon isothermal single-aging treatments was investigated at 732 °C and 621 °C. After this preliminary analysis, double-aging treatments were carried out changing the exposure times at both the primary aging temperature (732 °C) and the secondary aging one (621 °C). Hardness tests were performed in each aging condition investigated in this work. Successively, based on the hardness results, tensile and corrosion tests were carried out in a selection of aging conditions. SEM and EDXS analyses were performed to investigate the relationship between the microstructural constituents and the corrosion properties.

3. Results and Discussion

3.1. Soft-Annealed Condition

The as-forged material was soft-annealed at 1038 °C for 0.5 h in accordance with the ASTM B446-19 standard [6]. As reported in Figure 2, the austenitic microstructure showed the presence of equiaxed and twinned grains with a heterogeneous distribution of Nb-rich

carbides (grey color) and Ti-rich nitrides (orange color) dispersed in the matrix at both intergranular and intragranular positions. The average grain size measured according to the ASTM E112 standard was equal to 65 µm [25].



(**a**) (**b**)

Figure 2. LOM micrographs of the soft-annealed condition at different magnifications. (**a**) Presence of equiaxed and twinned austenite grains. (**b**) Presence of heterogeneously distributed Nb-rich carbides (grey color) and Ti-rich nitrides (orange color).

Then, the soft-annealed material was characterized by room-temperature tensile and hardness tests. The mechanical properties are reported in Table 2. The mechanical strength in the soft-annealed condition (350 MPa) is lower than the yield strength requirement required by the ASTM B446 standard (414 MPa) [6]. The insufficient mechanical properties are determined by grain coarsening during processing and heat treatment. As reported by Rivolta et al. [5], the larger the grain size, the lower the mechanical strength because of a reduction in the density of obstacles to the dislocation movements. In particular, the yield strength and the grain size measured in the soft-annealed condition are compatible with the relationship between these two properties reported in the literature for this alloy [5].

Table 2. Mechanical properties of the soft-annealed material determined by hardness and tensile tests at room temperature.

	Hardness	Yield Strength [MPa]	Ultimate Tensile Strength [MPa]	A%	Z%
This work	194 HV30	350	829	61.0	70
ASTM B446 [6]	---	>414	>827	>30.0	---

In the soft-annealed condition, the corrosion rate was equal to 0.65 mm/year, confirming the suitability of this heat treatment (1038 °C 0.5 h). The presence of Nb-rich MC carbides in the soft-annealed condition does not worsen the intergranular corrosion resistance, but it helps to improve it by stabilizing carbon.

3.2. Single-Aging Treatments

After soft annealing (1038 °C 0.5 h), the age-hardening effect was investigated with isothermal single-aging treatments at both 732 °C and 621 °C for up to 600 h starting from the results of a reduced set of conditions studied in our previous work [17]. The overall set of hardness data at both aging temperatures is reported in Figure 3 [17]. As shown in Figure 3, upon single aging at 621 °C, a steep hardness increase is obtained starting from 72 h. Until such exposure time, the hardness increment with respect to the soft-annealed condition is less than 10%. At 732 °C, the precipitation hardening effect is slightly higher compared to that at 621 °C, at least until the exposure times tested in this work. At 621 °C, a satisfying hardening effect is obtained only after very long exposure times and this behavior can limit its exploitation for most industrial applications. Such very slow age-hardening

kinetics is also confirmed by the literature data of Moore et al. and Suave et al. about single aging from 550 °C to 900 °C [8,15,16]. The hardness values of our work are compatible with the literature [15]. The age-hardening phenomenon in this temperature range is determined by precipitation of the γ'' phase, as shown in the TTP curves of Figure 1. According to the TTP curves, at these aging temperatures, the formation of intergranular $M_{23}C_6$ carbides can occur together with the intermetallic hardening γ'' precipitates. However, compared to the γ'' phase, the hardening effect of the $M_{23}C_6$ carbides is negligible [10]. The simultaneous formation of Cr-rich $M_{23}C_6$ carbides was deeply investigated by EDXS analyses performed by scanning electron microscopy. The IDs of the tested positions are reported in Figure 4 and the results of the EDXS analyses are given in Table 3 and Figure 5. At 732 °C, as shown in Table 3 and Figure 4, intergranular $M_{23}C_6$ carbides were not present until 1 h and the onset of their formation was detected in the 3 h sample. This observation is compatible with the literature data based on TEM examinations, as reported in the TTP diagram of Figure 1 [2]. According to the EDXS analyses reported in Table 3, the intergranular $M_{23}C_6$ carbides observed in the samples aged at 732 °C were mainly enriched in chromium, and this is also confirmed by the literature [2,9,10]. The formation of such carbides is expected to be significantly detrimental to the corrosion resistance.

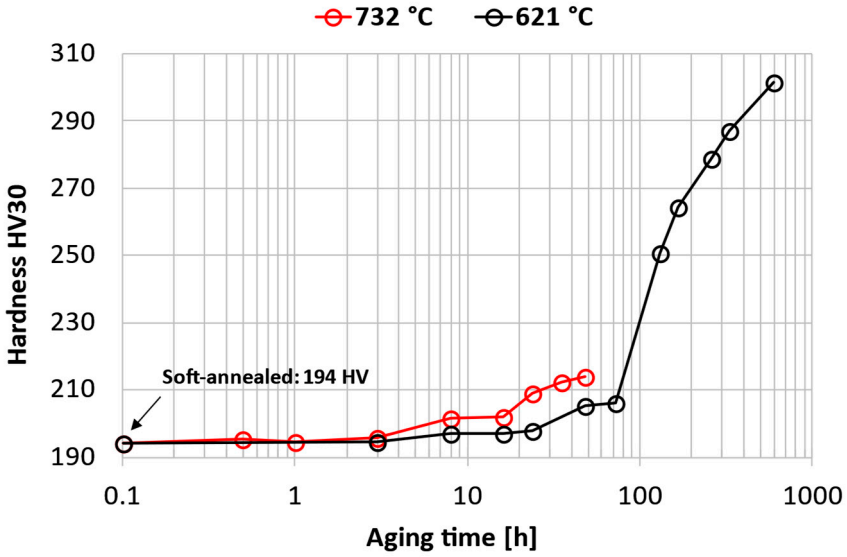
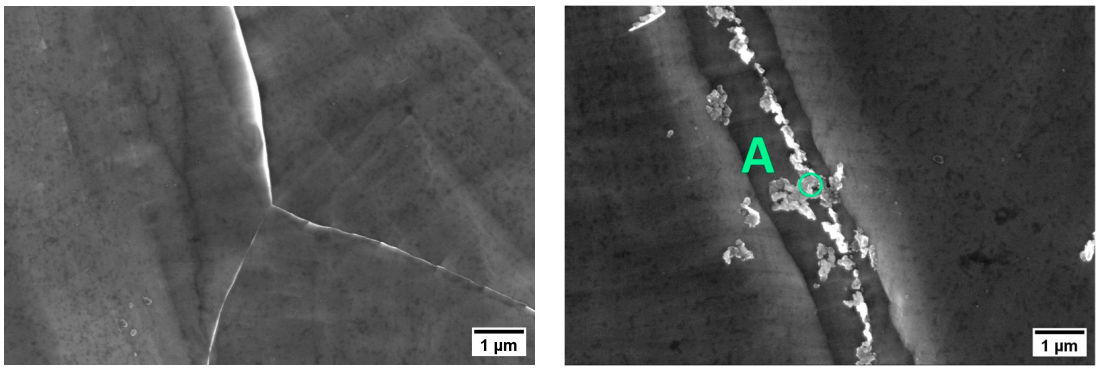
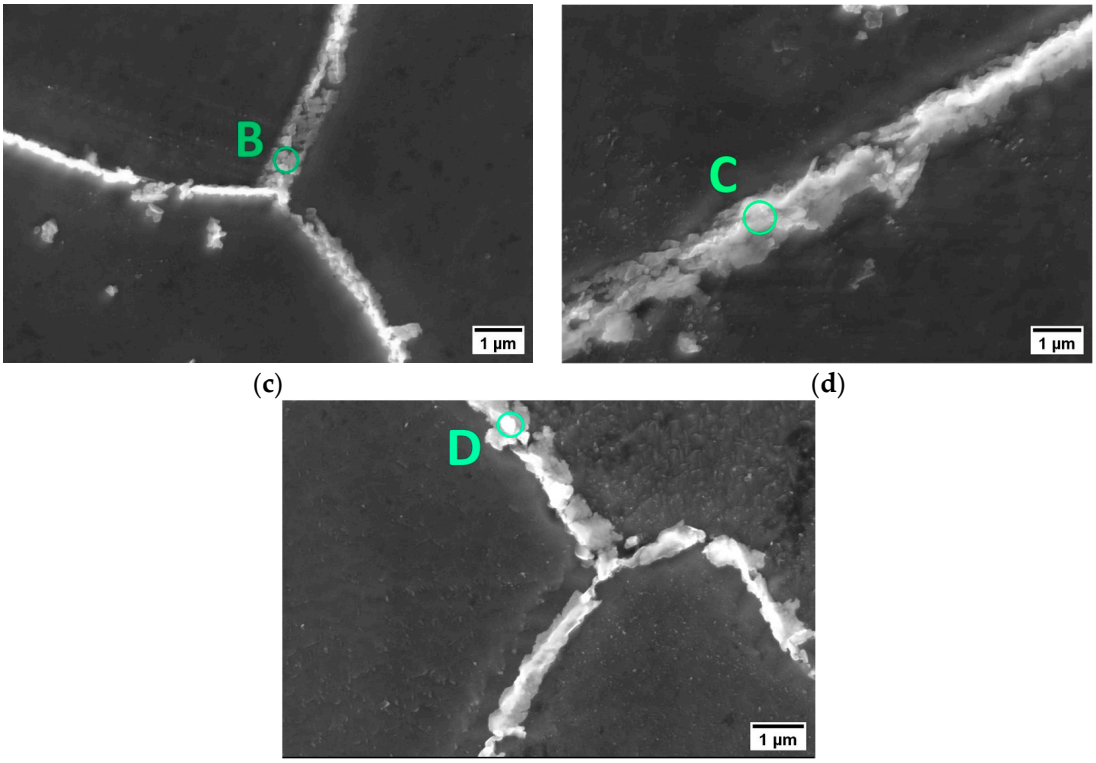


Figure 3. Hardness curves of the soft-annealed Alloy 625 after single-aging treatments.



(**a**) (**b**)

Figure 4. *Cont.*



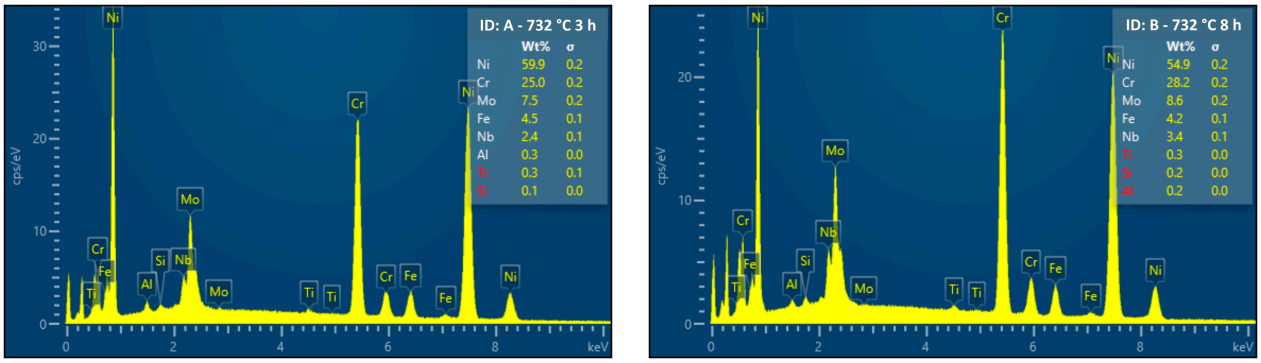
(**c**) (**d**)

(**e**)

Figure 4. SEM micrographs of the samples aged at 732 °C for different times: (**a**) 732 °C 1 h; (**b**) 732 °C 3 h; (**c**) 732 °C 8 h; (**d**) 732 °C 24 h; (**e**) 732 °C 48 h.

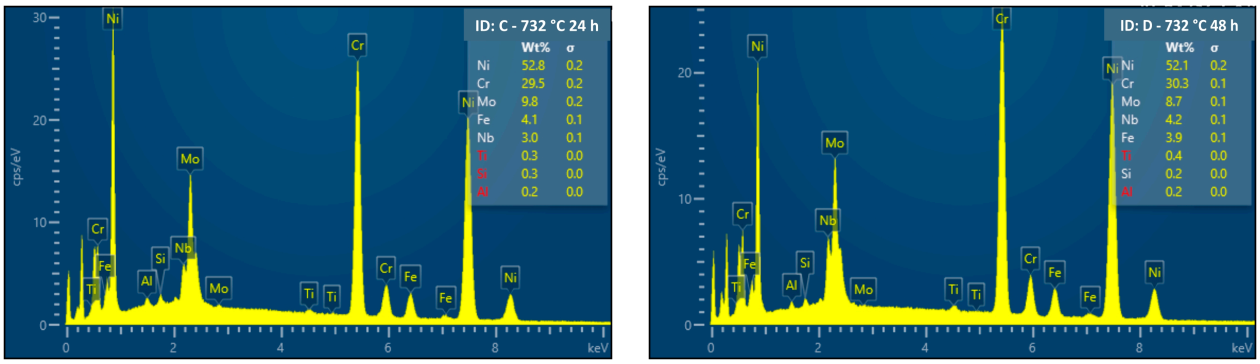
Table 3. EDXS analyses in wt. % at the positions reported in Figure 4.

	ID	Ni	Cr	Mo	Nb	Fe	Ti	Al	Si
OES analysis	---	62.3	20.4	8.50	3.59	4.41	0.30	0.20	0.17
Figure 4b	A	59.9	25.0	7.47	2.42	4.49	0.29	0.29	0.14
Figure 4c	B	54.9	28.2	8.60	3.40	4.20	0.30	0.20	0.20
Figure 4d	C	52.8	29.5	9.77	2.96	4.13	0.29	0.22	0.25
Figure 4e	D	52.1	30.3	8.75	4.22	3.89	0.37	0.17	0.20



(**a**) (**b**)

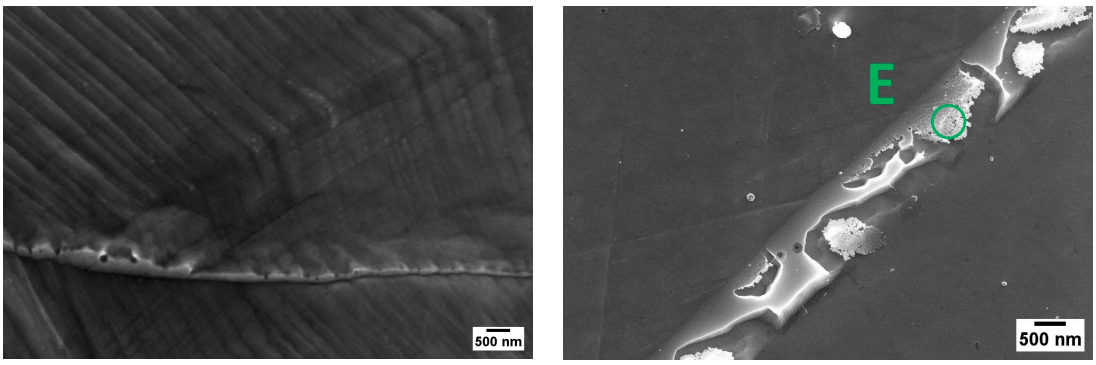
Figure 5. *Cont.*



(**c**) (**d**)

Figure 5. Spectra of the EDXS analyses reported in Table 3. (**a**) ID: A; (**b**) ID: B; (**c**) ID: C; (**d**) ID: D.

At 621 °C, the precipitation of the hardening γ'' phase is faster than that of the intergranular Cr-rich carbides. In fact, according to the TTP diagram of Figure 1, at this temperature, the formation of $M_{23}C_6$ carbides requires longer exposure times compared to 732 °C. This difference was confirmed by the SEM and EDXS analyses performed on the samples aged at 621 °C. The results are reported in Figure 6, Table 4, and Figure 7. In this work, Cr-rich $M_{23}C_6$ carbides were observed at the grain boundaries of the sample aged at 621 °C for 260 h, and they were not detected on shorter exposure times. So, upon aging at 621 °C, it is possible to exploit the precipitation of the hardening intermetallic γ'' phase before worsening the corrosion resistance.



(**a**) (**b**)

Figure 6. SEM micrographs of the samples aged at 621 °C for different times: (**a**) 621 °C 165 h; (**b**) 621 °C 260 h.

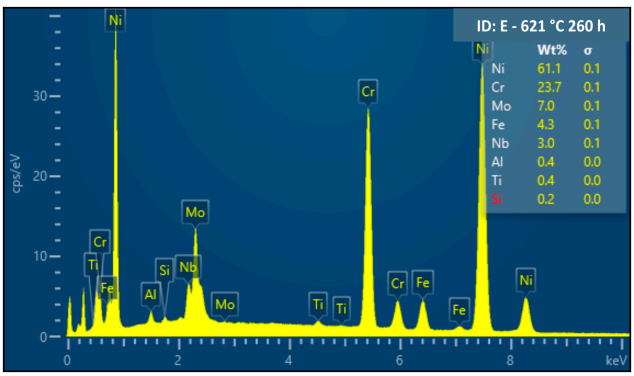


Figure 7. Spectrum of the EDXS analysis reported in Table 4 (ID: E).

Table 4. EDXS analysis in wt. % at the position reported in Figure 6.

	ID	Ni	Cr	Mo	Nb	Fe	Ti	Al	Si
OES analysis	---	62.3	20.4	8.50	3.59	4.41	0.30	0.20	0.17
Figure 6b	E	61.1	23.7	7.00	3.00	4.30	0.35	0.35	0.20

3.3. Double-Aging Treatments

After the investigation of the single-aging response, the possibility of accelerating the precipitation kinetics by double-aging treatments was studied considering different time-temperature conditions with primary aging at 732 °C (up to 48 h) and secondary aging at 621 °C (up to 592 h). The results are reported in Figure 8. According to the experimental observations, the double-aging treatments significantly accelerate the γ'' precipitation. In fact, fixing the duration of the secondary aging, the precipitation kinetic is accelerated, increasing the prior exposure time at 732 °C. In this case, short primary aging times are sufficient to obtain the peak hardness. The adoption of longer primary aging time is not associated with a further improvement in the mechanical strength. In fact, when the peak hardness is reached, the hardness curve remains almost flat. Considering the TTP diagram reported in Figure 1, the major drawback of such a double-aging procedure is represented by the primary aging temperature. In fact, even though the primary aging enables significant acceleration of the γ'' formation, such an aging temperature is also associated with a faster precipitation of intergranular carbides, which are extremely detrimental to the corrosion resistance. For this reason, it is required to limit as much as possible the primary aging exposure time. Regarding the double aging, Eiselstein and Tillack [1] found an increase in hardness from 170 HV to 210 HV adopting a primary treatment at 760 °C for 1 h prior to aging at 621 °C for 72 h. In our research work, the hardness increases from 195 HV to 280 HV with double aging at 732 °C for 1 h and 621 °C for 72 h. As described in the Introduction, this double-aging procedure was investigated starting from that of the alloy CarTech® Custom Age 625 PLUS® [18,19], for which the suggested double-aging treatment resulted in a hardness increase from 188 HV to 353 HV. Regarding our research work, the same heat treatment was associated with a poorer hardening response (from 194 HV to 220 HV) because of the lower titanium content.

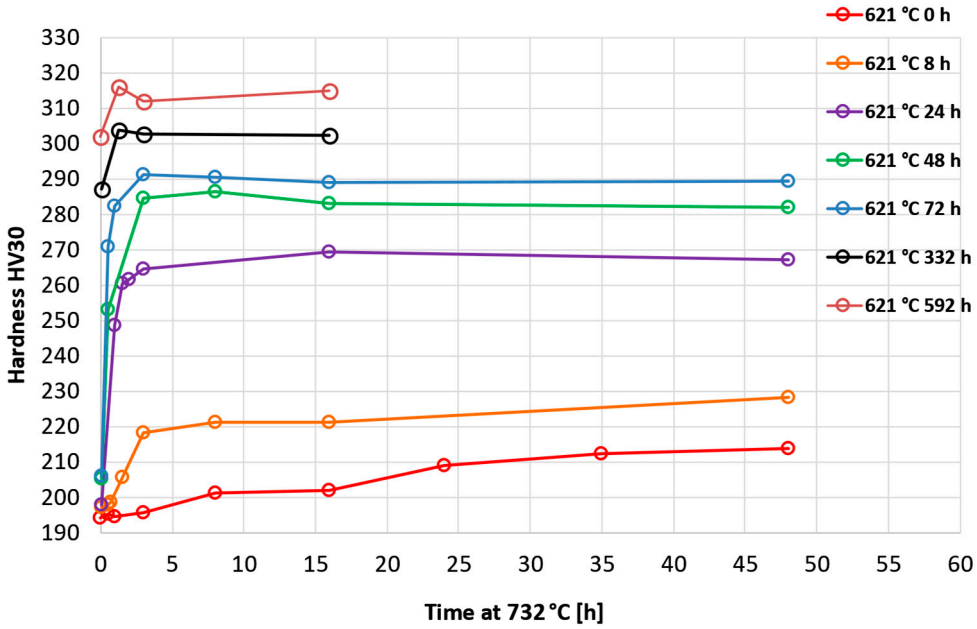


Figure 8. Double-aging Vickers hardness curves of the forged and soft-annealed Alloy 625 with different combinations of double-aging times at 732 °C and 621 °C.

Successively, in selected double-aging conditions, room-temperature tensile tests were performed. As shown in Figures 9 and 10, the tensile properties show a trend similar to that observed for the hardness curves reported in Figure 8. In fact, after a certain exposure time, the increase in the primary aging time with fixed secondary aging does not provide any further improvement for both the yield strength and the ultimate tensile strength. The hardening effect obtained by double aging is obtained at the expense of tensile deformability. In fact, a reduction in both A% and Z% was observed. However, the A% values remained well above the minimum standard requirement (30%) [6]. In all the tested double-aging conditions, except 732 °C 3 h plus 621 °C 8 h, both the yield strength and the ultimate tensile strength were compatible with the minimum standard requirements [6]. Therefore, when insufficient tensile properties characterize the soft- or solution-annealed condition, this aging procedure can be exploited to obtain satisfying strength improvements with reasonable heat treatment times compared to single aging. In fact, as previously described, compared to single-aging treatments, the double aging allows to significantly accelerate the hardening kinetic. As reported in Table 5, with double aging at 732 °C 3 h and 621 °C 72 h, it is possible to obtain the same mechanical properties of single aging at 621 °C for 260 h with a conspicuous acceleration of the aging response and consequent reduction in the heat treatment time and cost.

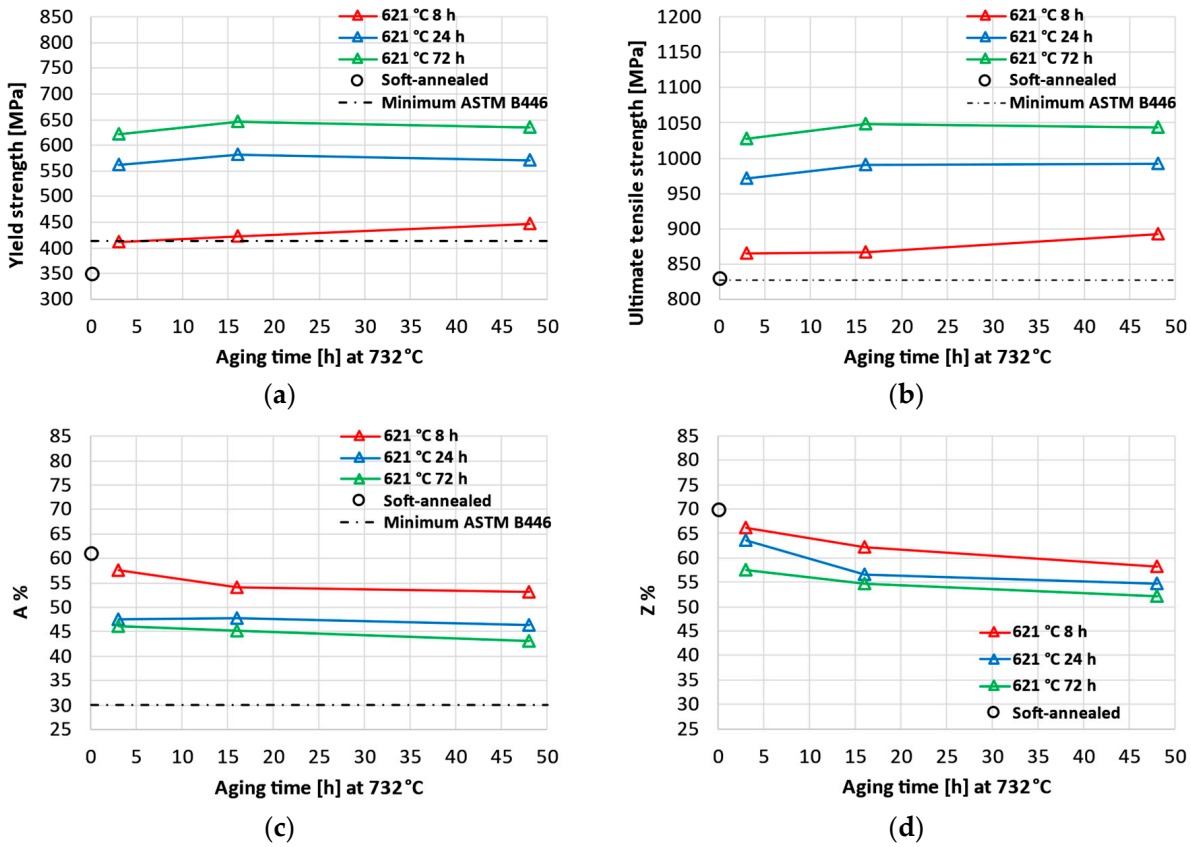


Figure 9. Room-temperature tensile properties in different double-aging conditions: (**a**) Rp0.2; (**b**) UTS; (**c**) A%; (**d**) Z%.

The possibility of estimating the tensile properties from the results of hardness tests represents a fast and useful tool in the analysis and comparison of different time–temperature aging conditions. The relationship between the hardness and the tensile strength was investigated by regression analysis of a dataset obtained combining the results reported in this work with those previously published in the literature [5,17]. The linear regression analysis of this larger set of experimental data is reported in Figure 11, together with the determination coefficient R^2, which was adopted to assess the goodness of fit. Considering

the results of this analysis and the requirements of the ASTM B446 standard [6], 192 HV and 202 HV represent the minimum hardness values for acceptable ultimate tensile strength and yield strength, respectively.

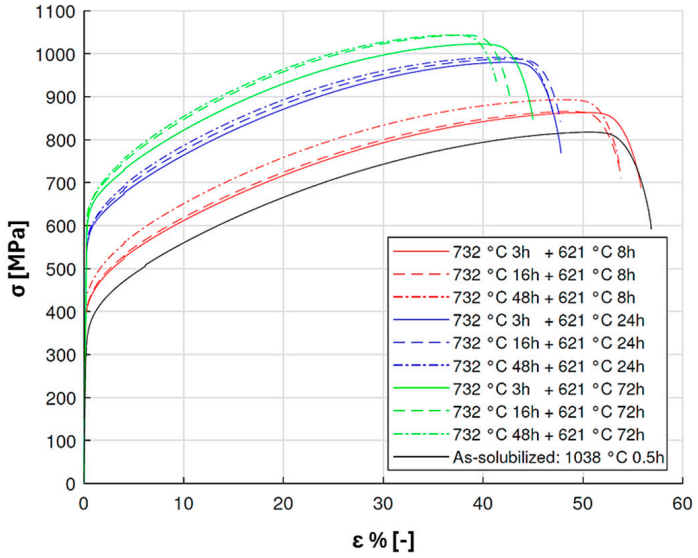


Figure 10. Stress–strain tensile curves of the aging conditions tested in this work.

Table 5. Comparison of the tensile properties upon single- and double-aging treatments with respect to the soft-annealed condition.

Condition	Hardness HV30	Yield Strength [MPa]	Ultimate Tensile Strength [MPa]	A%	Z%
Soft-annealed (SA)	194	350	829	61.0	70
SA + 621 °C 260 h	279	604	1039	46.0	62
SA + 732 °C 3 h + 621 °C 72 h	280	616	1023	47.0	57

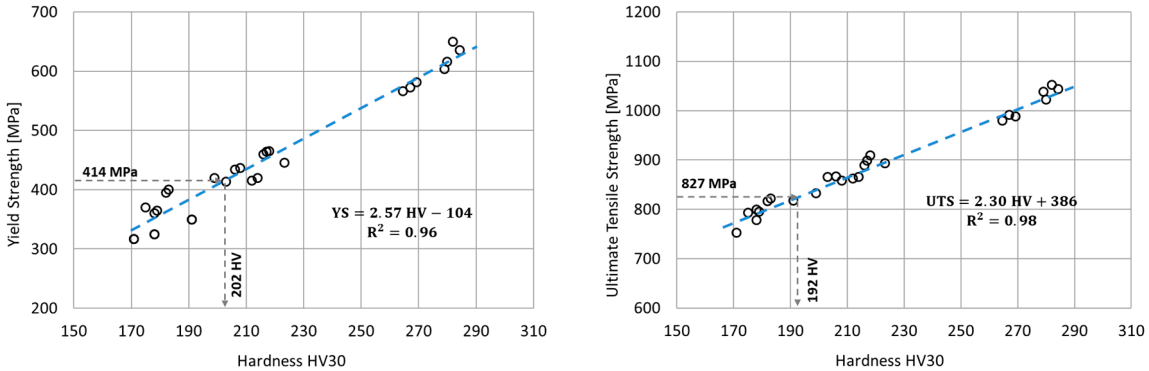


Figure 11. Relationship between the hardness and the tensile properties. (**a**) Relation between the hardness and the yield strength; (**b**) Relation between the hardness and the ultimate tensile strength. Dataset obtained with the results of this research work and those previously published in the literature. Adapted from Refs. [5,17].

3.4. Intergranular Corrosion Resistance

The intergranular corrosion resistance was analyzed in a selection of the conditions investigated in this work [20]. The variation in the corrosion rate as function of the aging time is depicted in Figure 12 for both single and double aging. The single-aging treatment

at 732 °C shows a rapid increment in the corrosion rate starting from 3 h and, until this exposure time, the hardening effect is very poor. This experimental result is confirmed by the SEM and EDXS analyses reported in Figure 4 and Table 3. In fact, single aging at 732 °C for 3 h represents the onset of intergranular Cr-rich carbide formation, which is known to be extremely detrimental to the corrosion resistance, as confirmed by the literature [10,26–29]. The rapid increase in the corrosion rate at longer exposure times is associated with a more copious formation of such carbides at the grain boundaries [26,28,30]. At 732 °C, such an undesired precipitation phenomenon occurs very quickly and the reduction in corrosion resistance becomes critical much earlier than the onset of γ'' precipitation, which represents the primary hardening phase. In fact, as confirmed by the experimental results and the literature [10,26,28], the hardening effect of the intergranular carbides is very poor and the effect of sensitization is predominant. At 621 °C, the precipitation of intergranular $M_{23}C_6$ carbides is obtained only after very long exposure times. This peculiarity allows us to exploit the hardening effect of the γ'' precipitates without worsening the corrosion resistance. Based on the experimental results reported in Figure 12, at 621 °C, the rapid increment in the corrosion rate is no longer obtained from 3 h as it occurs at 732 °C, but only after 130 h. Therefore, in this case, it is possible to exploit the hardening effect reported by the hardness curves in Figure 3 before worsening the intergranular corrosion resistance. This experimental result is confirmed by the SEM and EDXS analyses reported in Figure 6 and Table 4. Regarding the double aging, the corrosion tests were performed in selected conditions to evaluate the effect of an increasing primary exposure time at 732 °C with fixed secondary aging time. As shown in Figure 12, increasing the time at 732 °C, the corrosion resistance is quickly reduced because of a very rapid and copious precipitation of intergranular carbides. As shown by the results of the corrosion tests, the thermal exposure at 732 °C is surely the most critical and it should be restricted as much as possible to maintain the corrosion resistance within acceptable limits but provide sufficient acceleration of the precipitation response. Therefore, in the presence of double aging, the limitation of the primary aging time is extremely important also considering that above a certain duration there is no further strength improvement.

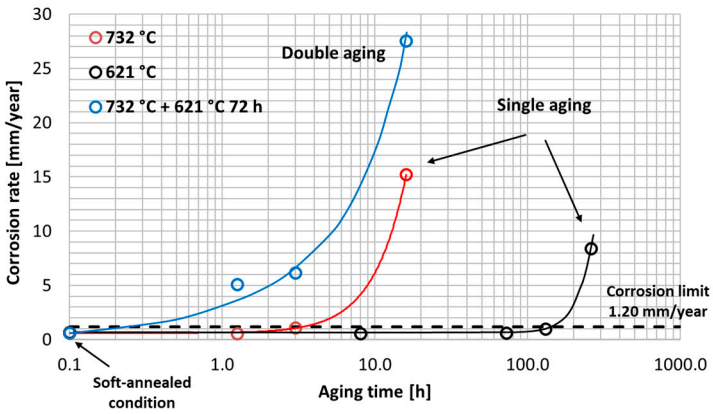


Figure 12. Corrosion rates obtained by intergranular corrosion tests (ASTM G28-A standard [20]) on different single- and double-aging conditions. Regarding the double-aging curve (732 °C + 621 °C 72 h), the aging time on the horizontal axis represents the primary aging time at 732 °C.

The corroded profiles were investigated in selected conditions to relate them with the calculated corrosion rates and characterize the corrosion mechanism. The optical micrographs shown in Figure 13 evidenced the presence of a selective corrosion of the grain boundaries. The intergranular sensitization upon both single- and double-aging treatment results from the precipitation at the grain boundaries of Cr-rich carbides, which deplete the surrounding regions of chromium, locally preventing the auto-passivation mechanism. Compared to single aging at 621 °C for 130 h (0.97 mm/year), the double aging with primary exposure at 732 °C for 16 h is responsible for a more copious precipitation of

Cr-rich carbides and consequently a more severe intergranular attack (26.4 mm/year), even associated with grains dropping. The calculated corrosion rates are in good agreement with the observed penetration depths.

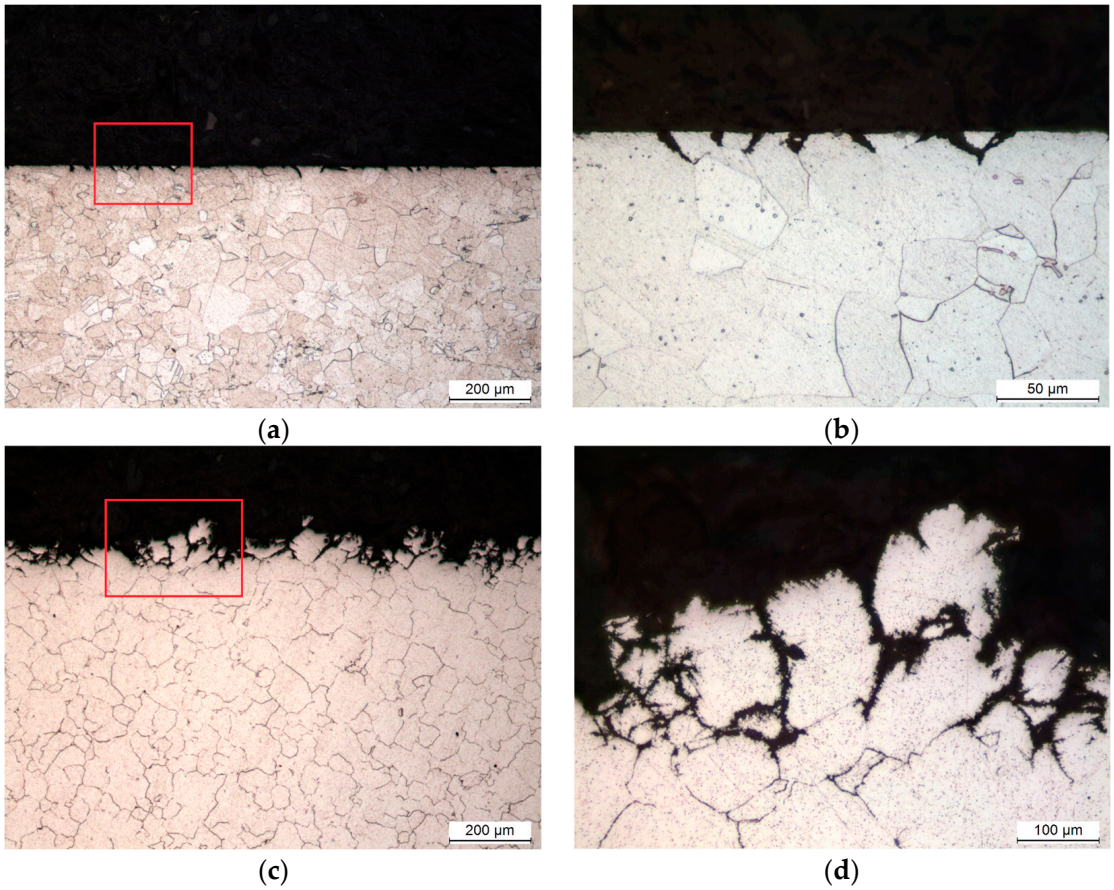


Figure 13. Morphologies of the corroded profiles at different magnifications upon single- and double-aging treatments: (**a**,**b**) 621 °C 130 h (0.97 mm/year); (**c**,**d**) 732 °C 16 h + 621 °C 72 h (26.4 mm/year). The red squares in (**a**) and (**c**) identify the regions highlighted at higher magnification in (**b**) and (**d**).

Considering the corrosion rate limit (1.20 mm/year) and the minimum requirement for the mechanical strength (202 HV), a performance map was built with the experimental conditions tested by hardness and corrosion tests in this work and in our previous paper [17], as shown in Figure 14. The hardness limit of 202 HV was calculated considering the minimum standard requirement for the mechanical strength [6] and the relationship between the hardness and the yield strength reported in Figure 11a. In the soft-annealed condition, only the corrosion resistance is acceptable. Single aging at 621 °C for 130 h provides good corrosion resistance and excellent mechanical strength. Longer aging times at 621 °C allow further strength improvement at the expense of a dramatic loss in the corrosion resistance. Regarding the double aging, even reducing the primary aging time down to 1 h, the corrosion rates remain above the threshold limit. In this case, a reduction in both the primary and secondary aging times is still not sufficient to obtain acceptable corrosion resistance. Moreover, further limitation of the primary aging exposure time would not be feasible in the presence of large components.

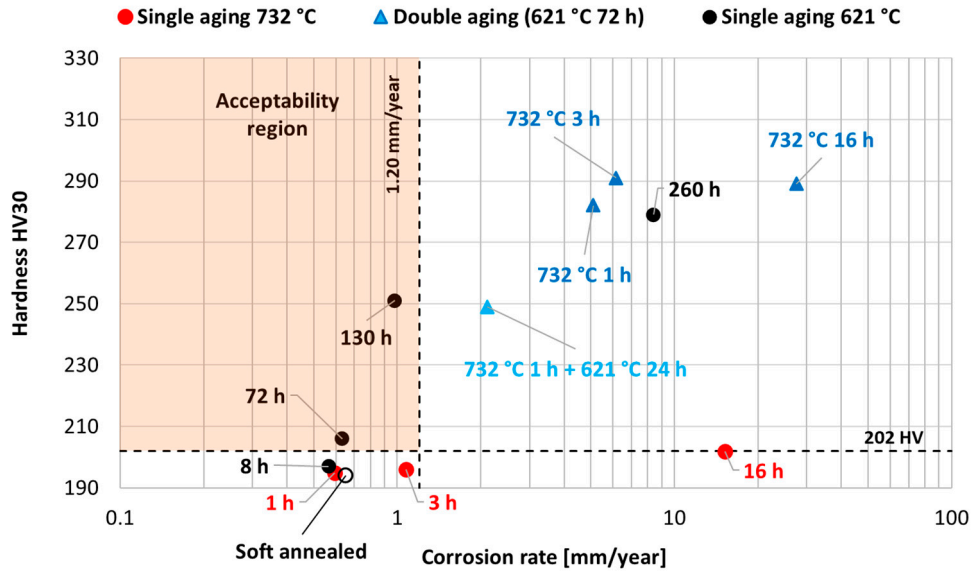


Figure 14. Experimental conditions of single and double aging tested in this work and in our previous paper. Adapted from Ref. [17]. The conditions positioned in the upper left quadrant with orange shading are acceptable based on the requirements for both the mechanical strength and the corrosion resistance.

4. Conclusions

Single- and double-aging treatments can be adopted to improve the mechanical strength of Alloy 625, especially when the soft-annealed condition is associated with insufficient mechanical properties. For instance, this possibility can be exploited to recover components characterized by excessive grain coarsening. The results obtained in this research work are summarized here:

(1) During aging treatments, the simultaneous formation of the hardening γ'' phase and intergranular Cr-rich carbides can detrimentally affect the corrosion resistance. Such undesired phenomenon occurs very quickly at 732 °C, but it is obtained only after very long exposure times at 621 °C. Therefore, this behavior allows us to better exploit the formation of the hardening γ'' phase at 621 °C before activating the precipitation of intergranular carbides.

(2) Single aging at 621 °C for 72 h and 130 h are associated with an acceptable combination of mechanical and corrosion properties. The corrosion resistance is instead not acceptable in the 260 h condition, where the mechanical properties are further improved.

(3) With double aging at 732 °C 3 h and 621 °C 72 h, it is possible to obtain the same mechanical properties of single aging at 621 °C for 260 h with a conspicuous acceleration of the aging response and consequent reduction in the heat treatment time and cost.

(4) The corrosion resistance remains a critical aspect in the case of double aging, especially because of the primary step. In this case, even after optimization of the primary aging time, none of the tested conditions was compatible with the imposed requirements. In addition, very short aging times cannot be feasible in the presence of large components.

Author Contributions: Conceptualization, B.R., R.G. and D.P.; Methodology, R.G. and D.P.; Formal Analysis, R.G. and D.P.; Investigation, B.R., R.G. and D.P.; Writing—Original Draft Preparation, D.P.; Writing—Review and Editing, B.R., R.G. and D.P.; Supervision, B.R. and R.G. All authors have read and agreed to the published version of the manuscript.

Funding: This research received no external funding.

Data Availability Statement: The raw data supporting the conclusions of this article will be made available by the authors on request.

Conflicts of Interest: The authors declare no conflicts of interest.

References

1. Eiselstein, H.L.; Tillack, D.J. The Invention and Definition of Alloy 625. In *Proceedings on Superalloys 718, 625, and Derivatives*; Loria, E.A., Ed.; The Minerals, Metals & Materials Society: Pittsburgh, PA, USA, 1991; pp. 1–14.
2. Floreen, S.; Fuchs, G.E.; Yang, W.J. The Metallurgy of Alloy 625. In *Superalloys 718, 625, 706 and Derivatives*; The Minerals, Metals & Materials Society: Pittsburgh, PA, USA, 1994; pp. 13–37.
3. Heubner, U.; Kloewer, J.; Alves, H.; Behrens, R.; Schindler, C.; Wahl, V.; Wolf, M. *Nickel Alloys and High-Alloyed Special Stainless Steels: Properties-Manufacturing-Applications*, 4th ed.; Expert-Verlag: Renningen, Germany, 2012.
4. Chen, X.; Nie, L.-Y.; Hu, H.; Lin, Y.C.; Liu, Y.-X.; Wu, Z.-L.; Zhou, X.; Zhang, J.; Lu, X. High-Temperature Deformation Characteristics and Constitutive Models of Inconel 625 Superalloy. *Mater. Today Commun.* **2022**, *32*, 103855. [CrossRef]
5. Rivolta, B.; Boniardi, M.V.; Gerosa, R.; Casaroli, A.; Panzeri, D.; Pizetta Zordão, L.H. Alloy 625 Forgings: Thermo-Metallurgical Model of Solution-Annealing Treatment. *J. Mater. Eng. Perform.* **2022**, *32*, 5785–5797. [CrossRef]
6. *ASTM B446-19*; Standard Specification for Nickel-Chromium-Molybdenum-Columbium Alloy (UNS N06625), Nickel-Chromium-Molybdenum-Silicon Alloy (UNS N06219), and Nickel-Chromium-Molybdenum-Tungsten Alloy (UNS N06650) Rod and Bar. ASTM International: West Conshohocken, PA, USA, 2019.
7. Reed, R.C.; Rae, C.M.F. Physical Metallurgy of the Nickel-Based Superalloys. In *Physical Metallurgy*; Elsevier: Amsterdam, The Netherlands, 2014; pp. 2215–2290. [CrossRef]
8. Suave, L.M.; Cormier, J.; Villechaise, P.; Soula, A.; Hervier, Z.; Bertheau, D.; Laigo, J. Microstructural Evolutions During Thermal Aging of Alloy 625: Impact of Temperature and Forming Process. *Metall. Mater. Trans. A* **2014**, *45*, 2963–2982. [CrossRef]
9. Yu, L.-J.; Marquis, E.A. Precipitation Behavior of Alloy 625 and Alloy 625 Plus. *J. Alloys Compd.* **2019**, *811*, 151916. [CrossRef]
10. Liu, X.; Fan, J.; Zhang, P.; Cao, K.; Wang, Z.; Chen, F.; Liu, D.; Tang, B.; Kou, H.; Li, J. Influence of Heat Treatment on Inconel 625 Superalloy Sheet: Carbides, γ″, δ Phase Precipitation and Tensile Deformation Behavior. *J. Alloys Compd.* **2023**, *930*, 167522. [CrossRef]
11. Sukumaran, A.; Gupta, R.K.; Anil Kumar, V. Effect of Heat Treatment Parameters on the Microstructure and Properties of Inconel-625 Superalloy. *J. Mater. Eng. Perform.* **2017**, *26*, 3048–3057. [CrossRef]
12. Heubner, U.; Köhler, M. The Effect of Final Heat Treatment and Chemical Composition on Sensitization, Strength and Thermal Stability of Alloy 625. In *Superalloys 718, 625, 706 and Derivatives*; The Minerals, Metals & Materials Society: Pittsburgh, PA, USA, 1997; pp. 795–803.
13. Liu, X.; Fan, J.; Jiao, D.; Tang, B.; Kou, H.; Sha, G.; Li, J. Achieving Excellent Strength-Ductility Combination in an Inconel 625 Superalloy via Short-Term Stress-Aging Treatment. *Scr. Mater.* **2023**, *231*, 115458. [CrossRef]
14. Yenusah, C.O.; Ji, Y.; Liu, Y.; Stone, T.W.; Horstemeyer, M.F.; Chen, L.-Q.; Chen, L. Three-Dimensional Phase-Field Simulation of Γ″ Precipitation Kinetics in Inconel 625 during Heat Treatment. *Comput. Mater. Sci.* **2021**, *187*, 110123. [CrossRef]
15. Moore, I.J.; Taylor, J.I.; Tracy, M.W.; Burke, M.G.; Palmiere, E.J. Grain Coarsening Behaviour of Solution Annealed Alloy 625 between 600–800 °C. *Mater. Sci. Eng. A* **2017**, *682*, 402–409. [CrossRef]
16. Suave, L.M.; Bertheau, D.; Cormier, J.; Villechaise, P.; Soula, A.; Hervier, Z.; Laigo, J. Impact of Microstructural Evolutions during Thermal Aging of Alloy 625 on Its Monotonic Mechanical Properties. *MATEC Web Conf.* **2014**, *14*, 21001. [CrossRef]
17. Rivolta, B.; Gerosa, R.; Panzeri, D.; Nazim, A. Optimization of the Mechanical and Corrosion Resistance of Alloy 625 through Aging Treatments. *Crystals* **2024**, *14*, 139. [CrossRef]
18. Carpenter Technology Corporation. CarTech® Custom Age 625 PLUS® Alloy: Technical Datasheet. Available online: www.carpentertechnology.com/alloy-finder/625-Plus (accessed on 25 August 2020).
19. Schmidt, N.B.; DeBold, T.A.; Frank, R.B. Custom Age 625® plus Alloy—A Higher Strength Alternative to Alloy 625. *J. Mater. Eng. Perform.* **1992**, *1*, 483–488. [CrossRef]
20. *ASTM G28-02*; Standard Test Methods for Detecting Susceptibility to Intergranular Corrosion in Wrought, Nickel-Rich, Chromium-Bearing Alloys. ASTM International: West Conshohocken, PA, USA, 2015.
21. ASM International. *ASM Specialty Handbook: Nickel, Cobalt, and Their Alloys*; Davis, J., Ed.; ASM International: Materials Park, OH, USA, 2000.
22. Carpenter Technology Corporation. A Guide to Etching Specialty Alloys for Microstructural Evaluation. Available online: https://carpentertechnology.com/blog/a-guide-to-etching-specialty-alloys (accessed on 14 November 2023).
23. *ISO 6507-1:2018*; Metallic Materials—Vickers Hardness Test. BSI Standards: London, UK, 2018.
24. *BS EN ISO 6892-1:2019*; Metallic Materials—Tensile Testing. BSI Standards Publication: London, UK, 2020.
25. *ASTM E112-13*; Standard Test Methods for Determining Average Grain Size. ASTM International: West Conshohocken, PA, USA, 2013. [CrossRef]
26. Hariharan, K.; Iams, A.D.; Zuback, J.S.; Palmer, T.A.; Sridhar, N.; Alazemi, R.M.; Frankel, G.S.; Schindelholz, E.J. Enhanced Localized Corrosion Resistance of Ni-Based Alloy 625 Processed by Directed Energy Deposition Additive Manufacturing. *Corros. Sci.* **2024**, *230*, 111945. [CrossRef]
27. Xue, J.; Guo, W.; Xia, M.; Zhang, Y.; Tan, C.; Shi, J.; Li, X.; Zhu, Y.; Zhang, H. In-Depth Understanding in the Effect of Hydrogen on Microstructural Evolution, Mechanical Properties and Fracture Micro-Mechanisms of Advanced High-Strength Steels Welded Joints. *Corros. Sci.* **2024**, *233*, 112112. [CrossRef]

28. Suthar, F.V.; Shah, H.N.; Mandal, D.; Chaudhury, S.K. Effect of Alloy 625 Buffer Layer on Corrosion Resistance of Nickel Base Hardfacing. *Surf. Coat. Technol.* **2024**, *485*, 130893. [CrossRef]
29. Liu, Z.; Gao, Z.; Song, J.; Guo, M.; Tian, Q.; Chen, P.; Lv, C.; Hu, W. Research on the Correlation between Tensile Ductility and Corrosion Behavior of Surfacing Alloy 625. *Mater. Charact.* **2024**, *208*, 113588. [CrossRef]
30. Zhu, J.; Feng, K.; Kokawa, H.; Li, Z. Effect of Heat Treatment on the Anisotropic Mechanical Properties and Corrosion Resistance of Laser Powder Bed Fusion Fabricated Inconel 625. *J. Alloys Compd.* **2024**, *1001*, 175087. [CrossRef]

Disclaimer/Publisher's Note: The statements, opinions and data contained in all publications are solely those of the individual author(s) and contributor(s) and not of MDPI and/or the editor(s). MDPI and/or the editor(s) disclaim responsibility for any injury to people or property resulting from any ideas, methods, instructions or products referred to in the content.